BNL-26165

CONF-791205--14

HEAT TRANSFER AND FLUID FLOW IN REGULAR ROD ARRAYS WITH OPPOSING FLOW*

J. W. Yang

Department of Nuclear Energy
Brookhaven National Laboratory
Upton, New York 11973

ABSTRACT

The heat transfer and fluid flow problem of opposing flow in the fully developed laminar region has been solved analytically for regular rod arrays. The problem is governed by two parameters: the pitch-to-diameter ratio and the Grashof-to-Reynolds number ratio. The critical Gr/Re ratios for flow separation caused by the upward buoyancy force on the downward flow were evaluated for a large range of P/D ratios of the triangular array. Numerical results reveal that both the heat transfer and pressure loss are reduced by the buoyancy force. Applications to nuclear reactors are discussed.

*Work performed under the auspices of the U.S. Department of Energy.

DISTRIBUTION OF THIS DOCUMENT IS UNLIMITED

DISCLAIMER

INTRODUCTION

It is well known that natural convection effects on heat transfer in rod arrays are important in many engineering applications. Due to the geometrical complexity of rod arrays, only a limited number of studies are reported in the literature. Most of the studies are related to the safety analysis of nuclear reactors and are applicable to specific reactors. Only a small part of the reported work includes the general characteristic geometry effects of the rod configuration on fluid flow and heat transfer. Iqbal et al. [1] first performed an analysis of the combined convection for infinite rod arrays of P/D (pitch-to-diameter ratio) between 1.3 and 2.5 with detailed results given for square arrays. Ramm and Johannsen [2] have extended the work of Iqbal et al. and applied it to a strip section of the hexagonal fuel assembly of an LMFBR (Liquid Metal Cooled Fast Breeder Reactor). The effects of radial power skews and duct wall heat transfer were included in their study. In both References [1] and [2], Nusselt numbers are evaluated in terms of the P/D ratio and the Rayleigh number based on the hydraulic diameter. Since the hydraulic diameter of a rod array depends on the P/D ratio, the two parameters are not mutually independent. The effects of buoyancy and P/D ratio cannot be treated separately. Recently, Yang [3] performed a detailed analysis for infinite triangular and square rod arrays. The results are governed by two independent parameters: the P/D ratio and the Rayleigh number based on the rod diameter. Thus, two parameters can be specified independently and the two effects, buoyancy and P/D ratio, can be evaluated separately. The work of Yang [3] and Iqbal et al. [1] is restricted to parallel flow, i.e., upward vertical flow. The opposing flow, i.e., downward vertical flow, is included in the studies of Ramm and Johannsen.

The opposing flow possesses unique features different from the parallel flow. In the opposing flow, the parabolic-type velocity profile is gradually

distorted due to deceleration of flow near rod surface as the buoyancy force increases. At high Rayleigh numbers, a point of inflection appears on the velocity profile and separation of flow occurs at the rod surface. According to the Rayleigh theorem, [4] this leads to flow instability. For nuclear reactors and many other industrial applications, flow stability is an important consideration in design and safety analysis.

In this paper, a detailed analysis of opposing flow in infinite rod arrays is performed. The velocity field, temperature field and the Nusselt numbers are investigated for a large range of pitch-to-diameter ratios and Rayleigh numbers. In addition, the critical Rayleigh number at which flow separation occurs is evaluated.

ANALYSIS

Physical models of the rod array are shown in Figure 1 for two basic arrangements. The equilateral triangular array commonly used in advanced nuclear reactors is used to show details of the analysis presented in this report. The square array is included in the mathematical formulation which can be evaluated for other applications.

For fully developed laminar flow in the vertical downward direction, the momentum and energy equations are:

$$\mu \nabla^2 u = - \rho g + \frac{dP}{dz} \tag{1}$$

$$K \nabla^2 t = \rho c_p u \frac{\partial t}{\partial z} \tag{2}$$

where

$$\nabla^2 = \frac{\partial^2}{\partial r^2} + \frac{1}{r}\frac{\partial}{\partial r} + \frac{1}{r^2}\frac{\partial}{\partial \phi}$$

In order to introduce the condition of fully developed heat transfer, it is assumed that the azimuthally-averaged heat transfer per unit length is uniform in the flow direction. Under these conditions, the axial temperature gradient is constant and an overall energy balance yields

$$\frac{\partial t}{\partial z} = \frac{dt_m}{dz} = \frac{q D \phi_o}{2\rho c_p u_m A_F} \tag{3}$$

The equation of state is assumed to be

$$\rho = \rho_w[1 - \beta(t - t_w)] \tag{4}$$

Substituting Equations (3) and (4) into Equations (1) and (2), and defining the new dimensionless velocity and temperature as U and T, respectively, one obtains

$$\nabla^2 U - \varepsilon^4 T = 1 \tag{5}$$

$$\nabla^2 T = U \tag{6}$$

where

$$R = 2r/D, \qquad T = \frac{8K A_F (t - t_w)}{D^3 \phi_o q E}$$

$$U = \left(\frac{u}{u_m}\right) / E, \quad E = \frac{D^2}{4\mu u_m}\left(\frac{dP}{dz} - \rho_w g\right)$$

and

$$\varepsilon = \left(\frac{Gr}{4\,Re}\right)^{1/4}, \quad Gr = \frac{g\,\beta\,\rho_w^2\,D^4\,q}{K\mu^2}, \quad Re = \frac{u_m D_h \rho_w}{\mu}$$

In Equations (5) and (6), the operator ∇^2 is defined in terms of the dimensionless coordinates R and ϕ. In carrying out the above transformations, the rod surface temperature, t_w, is assumed to be independent of angle, although it will vary along the length of rod. The boundary conditions are

$$U = 0, \quad T = 0 \qquad \text{at } R = 1 \tag{7}$$

$$\frac{\partial U}{\partial \theta} = 0, \quad \frac{\partial T}{\partial \theta} = 0 \qquad \text{at } \phi = 0 \text{ and } \phi_o \tag{8}$$

$$\frac{\partial U}{\partial \theta} = 0, \quad \frac{\partial T}{\partial n} = 0 \qquad \text{at } R = \frac{P/D}{\cos \phi} \tag{9}$$

The angle of symmetry, ϕ_o, is $\pi/6$ for the triangular array and $\pi/4$ for the square array. Equations (5) to (9) indicate that the system of opposing flow is governed by two dimensionless parameters: P/D (pitch-to-diameter ratio) and ε (ratio of the Grashof number and the Reynolds number). The parameter ε can be expressed in terms of the Rayleigh number based on the rod diameter:

$$\varepsilon = \left(\frac{\pi\, Ra_D}{96\ \phi_o}\right)^{1/4}, \qquad \text{where } Ra_D = \frac{\beta\, g\, \rho_w^2\, c_p\, D^4}{K\mu}\left(\frac{\partial t}{\partial z}\right)$$

Thus, the two parameters can be specified independently and the effect of buoyancy can be evaluated for various pitch-to-diameter ratios.

In order to obtain the general solution of Equations (5) and (6), the two equations are combined to give

$$\nabla^4 U - \varepsilon^4 U = 0 \tag{10}$$

or

$$(\nabla^2 - \varepsilon^2)(\nabla^2 + \varepsilon^2)U = 0 \tag{11}$$

General solutions of Equation (11) are obtained by combining solutions of

$$\nabla^2 U - \varepsilon^2 U = 0 \tag{12}$$

and

$$\nabla^2 U + \varepsilon^2 U = 0 \tag{13}$$

Using the standard method of separation of variables, it can be shown that the solution of Equation (12) contains terms of

$$I_m(\varepsilon R)\cos m\phi, \quad I_m(\varepsilon R)\sin m\phi, \quad K_m(\varepsilon R)\cos m\phi, \quad K_m(\varepsilon R)\sin m\phi;$$

and the solution of Equation (13) contains

$$J_m(\varepsilon R)\cos m\phi, \quad J_m(\varepsilon R)\sin m\phi, \quad Y_m(\varepsilon R)\cos m\phi, \quad Y_m(\varepsilon R)\sin m\phi.$$

According to boundary condition (8), the problem is even in ϕ and all terms containing $\sin m\phi$ will drop out. In addition, the constant m will be positive integers, i.e.,

m = 0, 6, 12, 18, 24, ... for triangular arrays

m = 0, 4, 8, 12, 16, ... for square arrays

Thus, the general solution for U becomes

$$U = \sum_m \Big[A_m I_m(\varepsilon R) + B_m K_m(\varepsilon R) + C_m J_m(\varepsilon R) + D_m Y_m(\varepsilon R)\Big]\cos m\phi \tag{14}$$

The corresponding solution for T is obtained from Equations (5), (12) and (13),

$$T = \frac{1}{\varepsilon^2}\sum_m \Big[A_m I_m(\varepsilon R) + B_m K_m(\varepsilon R) - C_m J_m(\varepsilon R) - D_m Y_m(\varepsilon R)\Big]\cos m\phi - \frac{1}{\varepsilon^4} \tag{15}$$

The four sets of constants A_m, B_m, C_m, and D_m are determined from Equations (7) and (9) by using the point matching method. [5] Applying the boundary conditions, Equations (7) and (9) to Equations (14) and (15), yields four sets of algebraic equations which can be readily solved.

The parameter E (the pressure loss term) is determined from the continuity equation:

$$u_m A_F = \int_o^{\phi_o} \int_{D/2}^{P/2\cos\phi} u\, r\, dr\, d\phi \tag{16}$$

which yields

$$E = \frac{4 A_F}{D^2} \left[\int_o^{\phi_o} \int_1^{\frac{P/D}{\cos\phi}} U\, R\, dR\, d\phi \right]^{-1} \tag{17}$$

Knowing the parameter E, the complete velocity and temperature fields are thus determined.

The wall-to-bulk temperature difference and the Nusselt number are generally the results of practical importance. They can be computed from the complete velocity and temperature solutions. The wall-to-bulk temperature difference is defined as

$$t_m - t_w = \frac{\int_{A_F}\int u(t - t_w)\, r\, dr\, d\phi}{\int_{A_F}\int u\, r\, dr\, d\phi}$$

or, in dimensionless form

$$T_m = \frac{E^2 D^2}{4 A_F} \int_o^{\phi_o} \int_1^{\frac{P/D}{\cos\phi}} U\, T\, R\, dR\, d\phi \tag{18}$$

The integrand was evaluated numerically from the velocity and temperature solutions given by Equations (14) and (15). The Nusselt number is defined as

$$Nu = \frac{q D_h}{K(t_w - t_m)}$$

Introducing the dimensionless temperature, one obtains

$$Nu = -\left(\frac{D_h}{D}\right)^2 \Big/ T_m$$

or

$$Nu = -\left[\frac{2\sqrt{3}}{\pi}\left(\frac{P}{D}\right)^2 - 1\right]^2 \Big/ T_m \qquad \text{for triangular array} \qquad (19)$$

$$Nu = -\left[\frac{4}{\pi}\left(\frac{P}{D}\right)^2 - 1\right]^2 \Big/ T_m \qquad \text{for square array} \qquad (20)$$

RESULTS

The effect of buoyancy on the radial velocity distribution is illustrated in Figure 2 for a P/D ratio of 1.5. Two sets of velocity profiles at $\phi=0$ (gap region) and $\phi=30^{o}$ (central region) are included in Figure 2. As expected, the parabolic-type velocity profiles at low Gr/Re ratio (curve 1) are distorted by the buoyancy force with the increase of Grashof numbers (curves 2 and 3). Comparison of the two sets of velocity profiles reveals that the buoyancy force has a much stronger effect on flow in the gap region (i.e., $\phi=0$). In this region, the downward flow velocity is considerably retarded by the upward buoyancy force. Consequently, in the central region at $\phi=30^{o}$, the flow is accelerated by the buoyancy effect in order to satisfy continuity of total mass flow rate. It is seen that at sufficiently high Gr/Re ratios, the flow is so retarded that flow reversal occurs near the rod surface at the gap region (curve 3). The corresponding temperature profiles at both the gap and central regions are shown in Figure 3. Contrary to the velocity profiles, the temperature profiles are not strongly affected by the upward buoyancy force imposed on the flow field.

Representative graphs of the buoyancy effect on rod arrays with various pitch-to-diameter ratios are shown in Figure 4. Similar to the parallel flow in the rod arrays given in Reference [4], the buoyancy force exhibits a larger effect with an increase in pitch-to-diameter ratio. For rod arrays of large P/D ratio, i.e., large flow area between rods, there is a great tendency for the upward buoyancy force to slow down the fluid near the rod surface and to accelerate the fluid near the central region. The deceleration of flow near the rod surface, illustrated in Figures 2 and 4, indicates the unique feature of the opposing flow. At high Gr/Re ratios, the upward buoyancy force will cause a point of inflection on the velocity profiles of the downward flow. This results

in flow separation at the rod surface and leads to flow instability as described by the Rayleigh theorem. [4] Numerical computations were carried out to evaluate the critical Gr/Re ratios at which the velocity gradient at the rod surface vanishes. It is considered in this study that the zero velocity gradient leads to separation of flow from the rod surface and causes flow instability. Detailed computations show that for all P/D ratios between 1.1 and 1.5, the velocity gradient first vanishes at $\phi=0^{o}$ as the Grashof-Reynolds number ratio is increased. The critical Gr/Re ratios for the first occurrence of flow separation (i.e., at $\phi=0^{o}$) are plotted in Figure 5 where it is seen that rod arrays with smaller P/D ratios are more stable than arrays with larger P/D ratios. The increase of the critical Gr/Re ratio at smaller P/D ratios agrees with the velocity profiles shown in Figure 4.

The critical Gr/Re curve in Figure 5 provides some interesting insights on the applications to nuclear reactors. For advanced fast reactors, such as the Gas-Cooled Fast Reactor (GCFR) and Liquid-Metal Cooled Fast Breeder Reactor (LMFBR), representative P/D ratios in the fuel assembly are 1.35 and 1.25, respectively. At these pitch-to-diameter ratios, expected Gr/Re ratios for these nuclear reactors under off-normal conditions with reduced flow rate are much less than the estimated critical Gr/Re ratios in Figure 5. Thus, it seems that the buoyancy force is unlikely to cause flow instability for current designs of nuclear reactors.

Finally, the Nusselt number and the pressure drop results are shown in Figures 6 and 7, respectively. In Figure 6, the asymptotic Nusselt numbers are compared with the Nusselt numbers of purely forced convection (Reference [5]) and good agreement is indicated. As the Gr/Re ratio is increased, the Nusselt number decreases slowly in a manner similar to that observed in circular pipes

with opposing flow. [6] When the Gr/Re ratio becomes sufficiently large and the flow is considerably retarded, the Nusselt number is then reduced rapidly, as indicated in Figure 6. For nuclear reactors within the expected range of the Gr/Re ratio, the Nusselt numbers are not significantly affected by the buoyancy force. Thus, the heat transfer computed from correlations based on forced convection flow can still be applied for the combined convection flow.

The pressure parameter E is plotted in Figure 7. The pressure parameter exhibits a very large dependence on the Gr/Re ratio as the buoyancy force is increased similar to the Nusselt number. With no buoyancy force, the parameter E is negative (i.e., flow is in a favorable pressure field and dP/dz is negative). With the increase of buoyancy force, the flow becomes retarded and the pressure gradient is reduced. At high Gr/Re ratios, the pressure gradient becomes positive and eventually the parameter E is positive, as indicated in Figure 7. The adverse pressure gradient is closely related to the process of flow separation, as described by the boundary layer theory. [4] Thus, the pressure parameter E, in Figure 7, also indicates the approach of flow separation at high Gr/Re ratios.

CONCLUSION

The problem of opposing flow in regular rod arrays is investigated under various conditions. Numerical results of the velocity field, temperature field, Nusselt number and pressure drop are performed for triangular arrays. The critical Gr/Re ratio for flow separation is evaluated. For nuclear reactors within the expected range of Gr/Re ratio, the flow is in the stable region and the heat transfer is slightly affected by the buoyancy force.

REFERENCES

1. Iqbal, M., Ansari, S. A. and Aggarwala, B. D., "Buoyancy Effects in Longitudinal Laminar Flow Between Vertical Cylinders Arranged in Regular Arrays," Heat Transfer 1970 (Proc. 3rd Intern. Heat Transfer Conf.), Vol. IV, NC 3.6.

2. Ramm, H. and Johannsen, K., "Combined Forced and Free Laminar Convection in Vertical Rod Bundles with Longitudinal Flow," ASME Paper 77-HT-44, 1977.

3. Yang, J. W., "Analysis of Combined Convection Heat Transfer in Infinite Rod Arrays," Heat Transfer 1978 (Proc. 5th Intern. Heat Transfer Conf.), Vol. I, p. 49.

4. Schlichting, H., Boundary-Layer Theory, McGraw-Hill, 1960.

5. Sparrow, E. M., Loeffler, A. L. Jr., and Hubbard, H., "Heat Transfer to Longitudinal Laminar Flow Between Cylinders," Journal of Heat Transfer, Trans. ASME, Series C, Vol. 83, p. 415 (1961).

6. Hanratty, T. J., Rosen, E. M. and Kabel, R. L., "Effect of Heat Transfer on Flow Field at Low Reynolds Numbers in Vertical Tubes," Ind. and Eng. Chem., Vol. 50, p. 815 (1958).

NOMENCLATURE

A_F = coolant flow area

c_p = specific heat at constant pressure

D = rod diameter

D_h = hydraulic diameter

E = dimensionless pressure loss

g = acceleration of gravity

Gr = Grashof number

K = thermal conductivity

Nu = Nusselt number

p = pressure

P = pitch of rod array

q = heat flux

r = radial coordinate

R = dimensionless radial coordinate

Re = Reynolds number

t = temperature

T = normalized temperature

t_m = fluid mean temperature

u = axial velocity

U = normalized velocity

u_m = fluid mean velocity

z = axial coordinate

NOMENCLATURE (cont.)

β = volume expansion coefficient

ϵ = ratio of Grashof number to Reynolds number

ϕ = angular coordinate

ϕ_o = angle of symmetry

μ = viscosity

ρ = density

LIST OF FIGURES

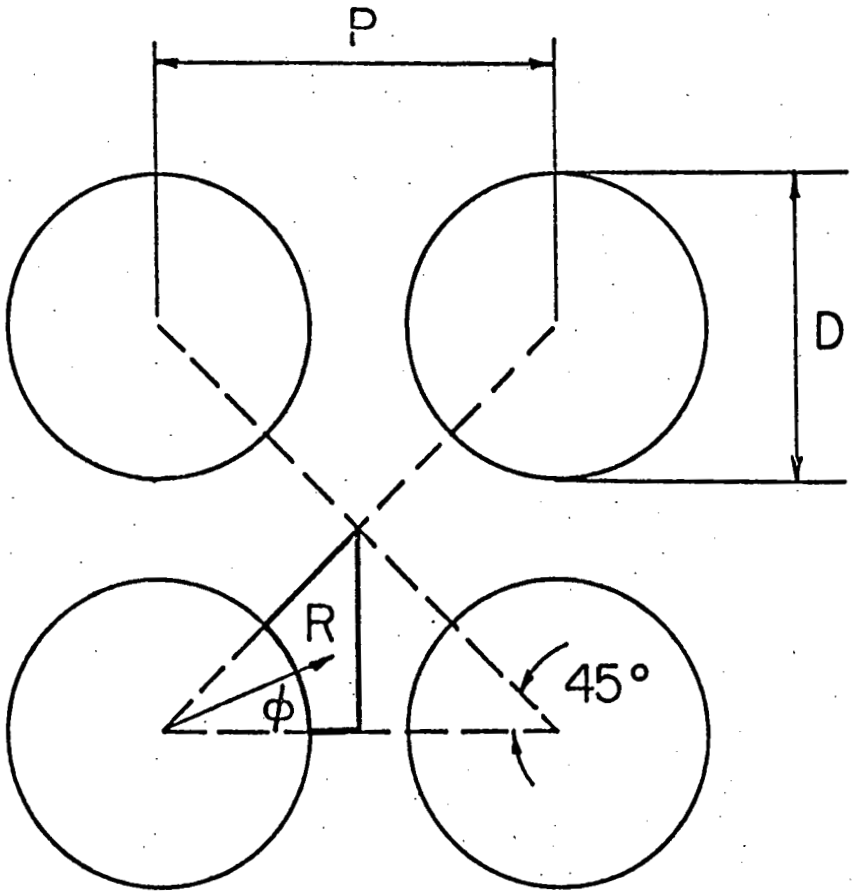

SQUARE ARRAY

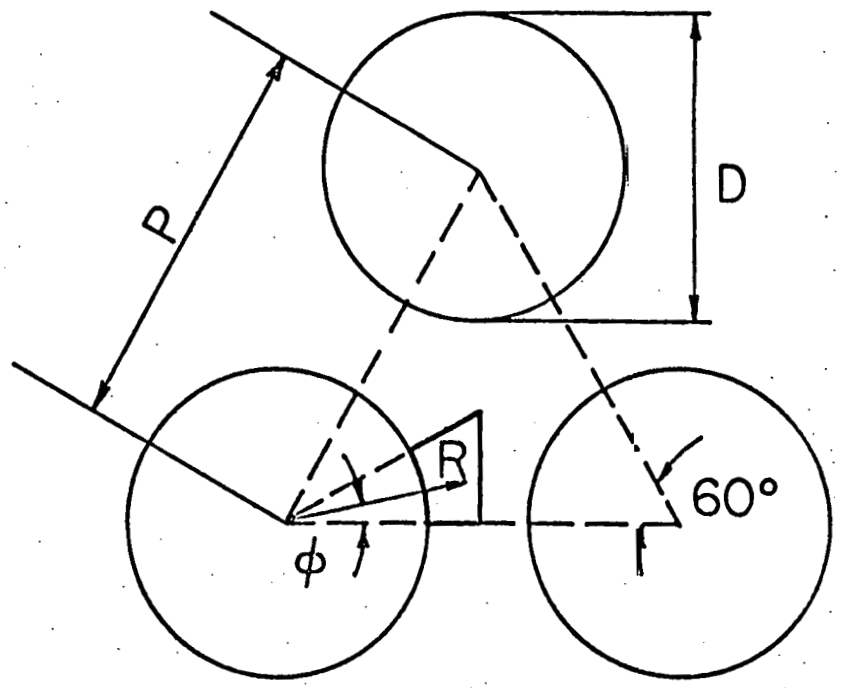

TRIANGULAR ARRAY

Fig. 1

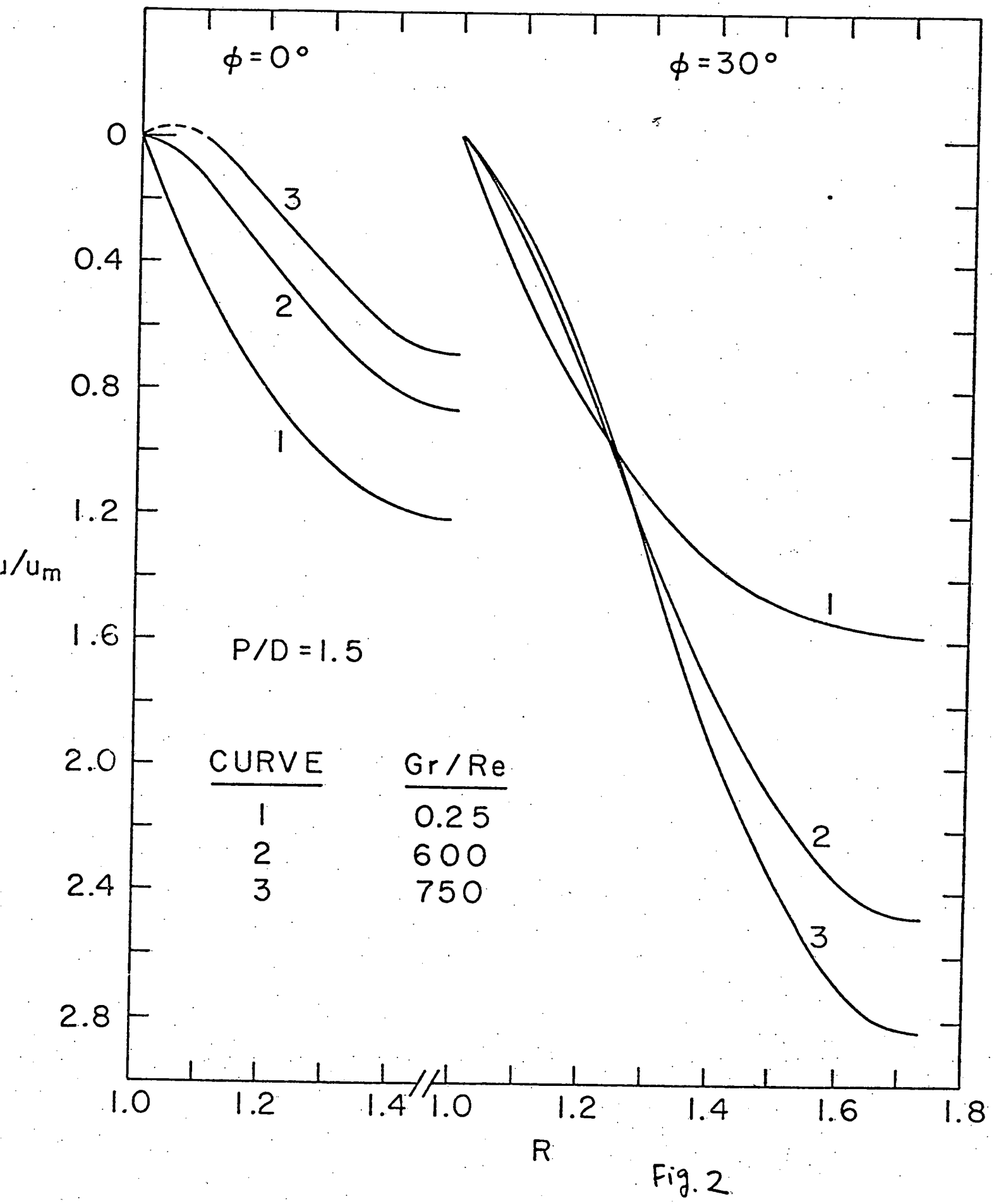
φ = 0°
φ = 30°
0
0.4
0.8
1.2
1.6
2.0
2.4
2.8
u/u_m
3
2
1
1
2
3
P/D = 1.5
CURVE
Gr/Re
1
0.25
2
600
3
750
1.0
1.2
1.4
1.0
1.2
1.4
1.6
1.8
R

Fig. 2

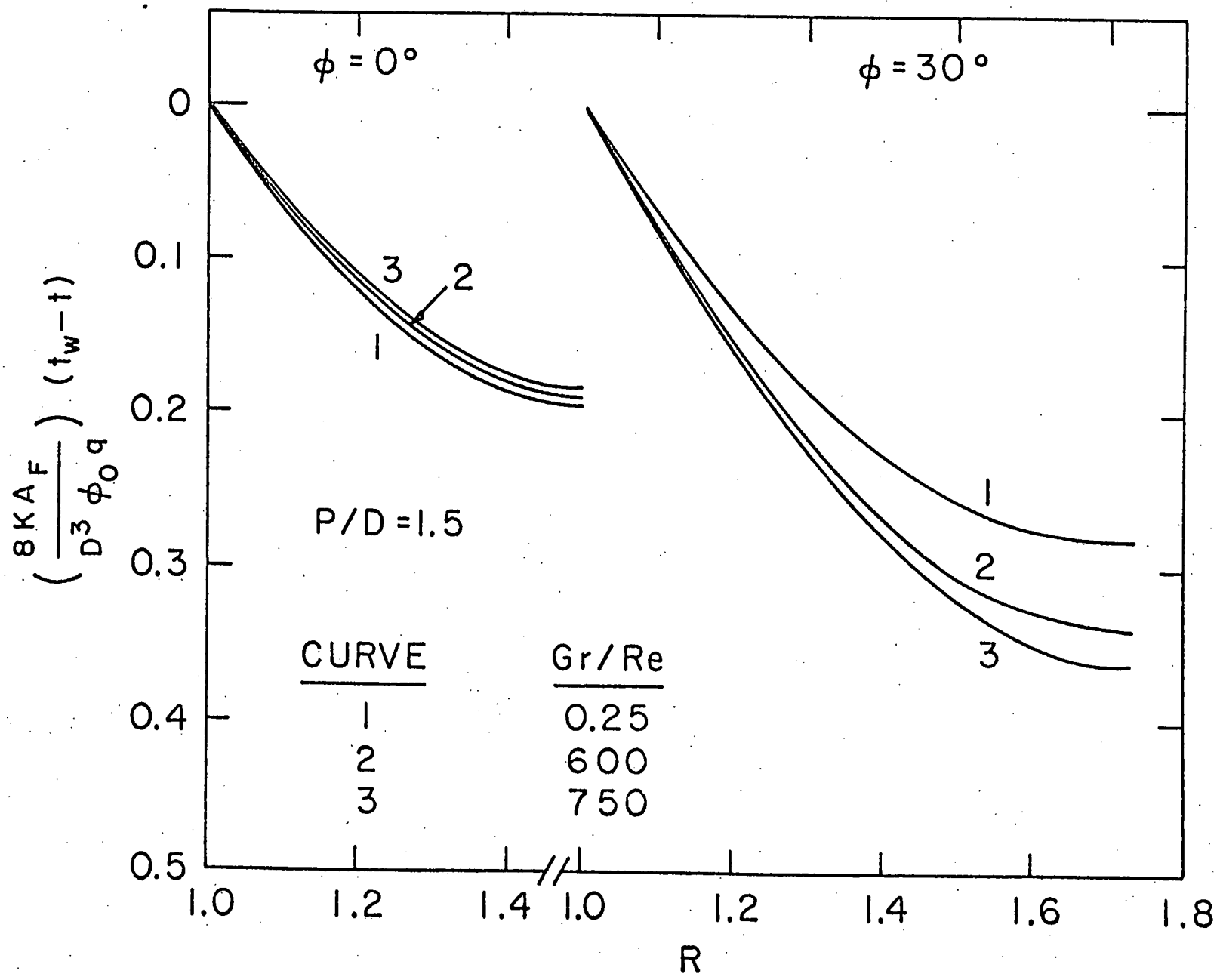
$\phi = 0°$
$\phi = 30°$
$\left(\frac{8KA_F}{D^3\phi_0 q}\right)(t_w - t)$
0
0.1
0.2
0.3
0.4
0.5
P/D = 1.5
CURVE
Gr/Re
1
0.25
2
600
3
750
1.0
1.2
1.4
1.0
1.2
1.4
1.6
1.8
R

Fig. 3

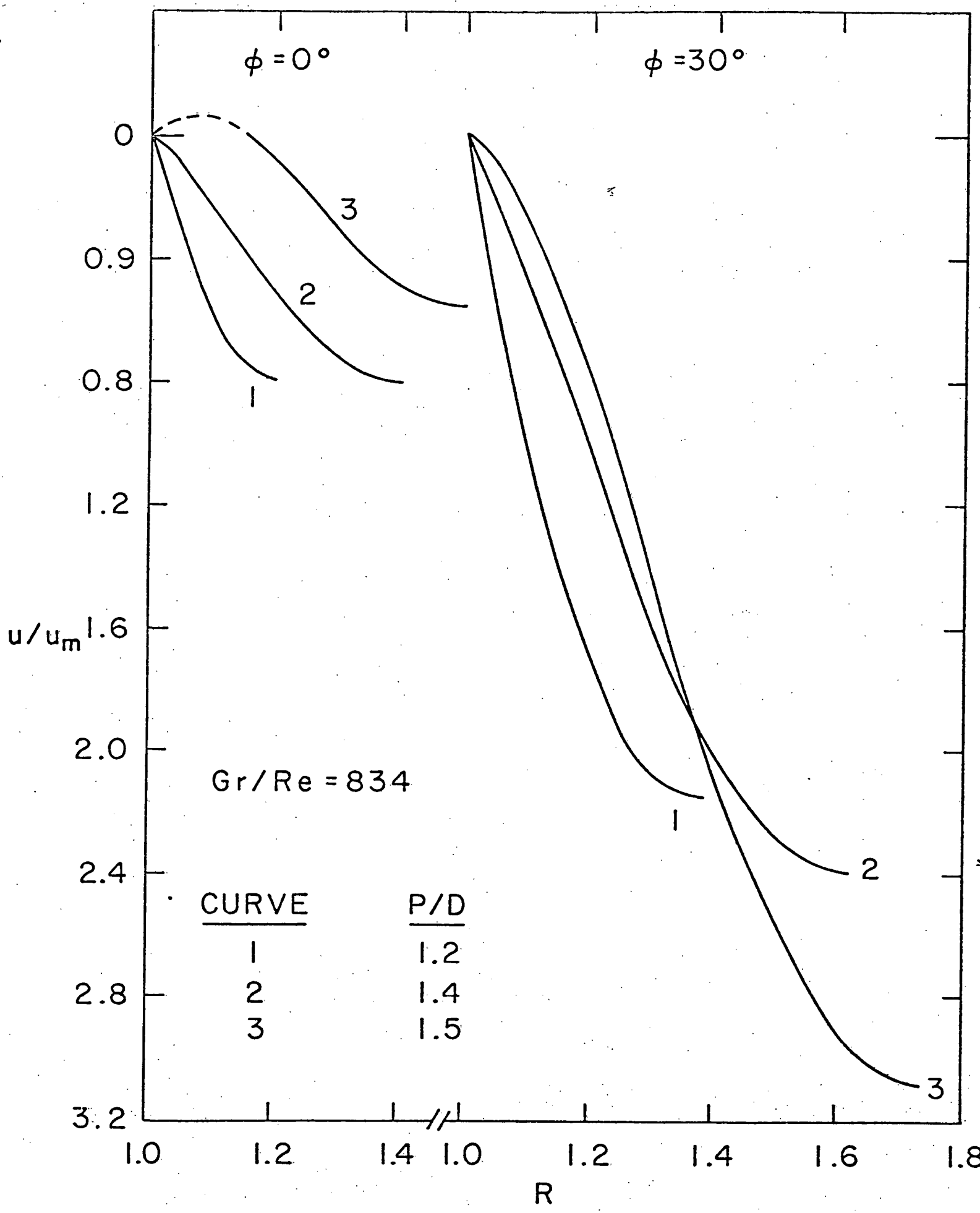
φ = 0°
φ = 30°
0
0.9
0.8
1.2
1.6
2.0
2.4
2.8
3.2
u/u_m
1
2
3
Gr/Re = 834
CURVE P/D
1 1.2
2 1.4
3 1.5
1.0
1.2
1.4
1.0
1.2
1.4
1.6
1.8
R

Fig 4.

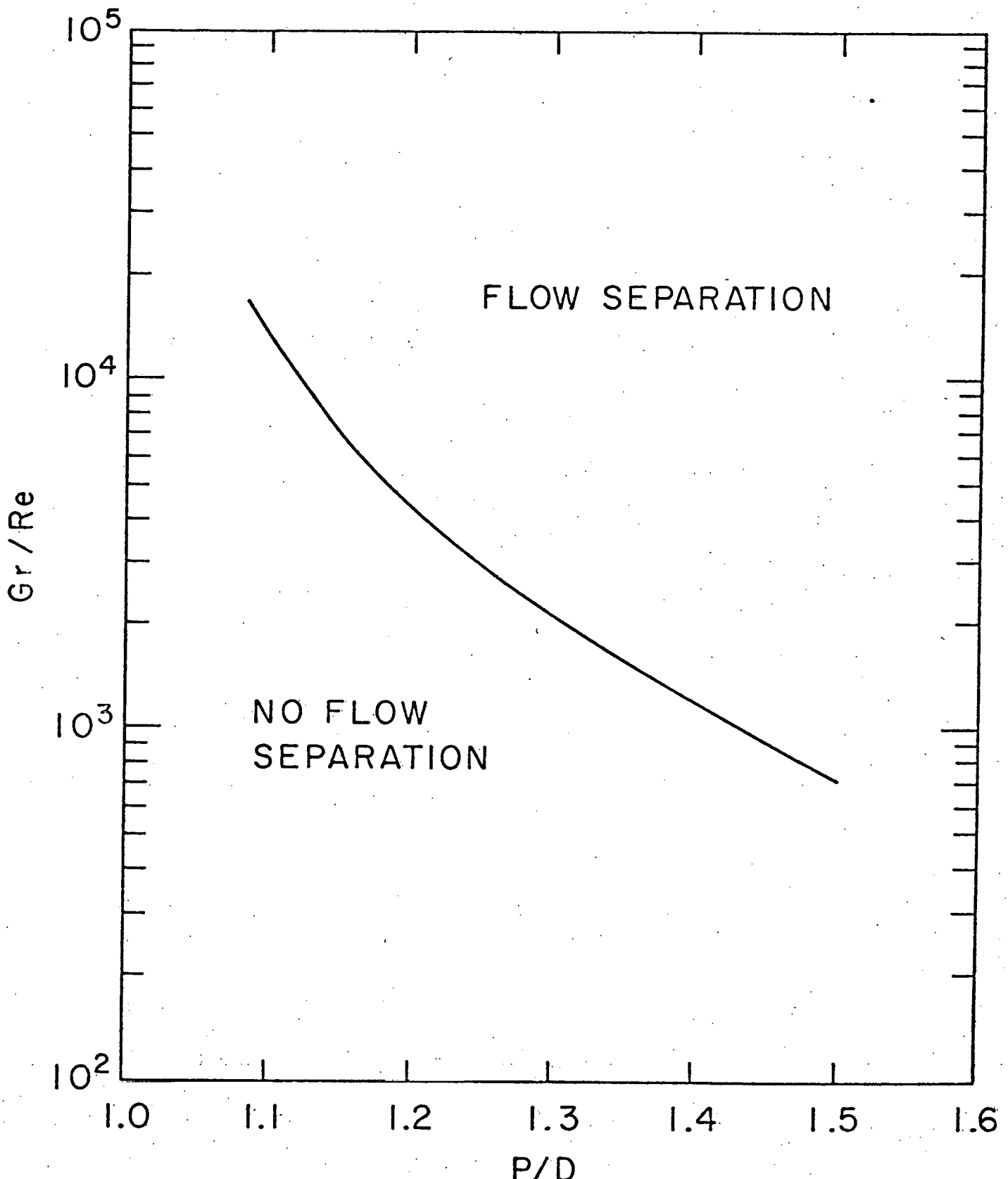
10^5
10^4
10^3
10^2
Gr/Re
FLOW SEPARATION
NO FLOW
SEPARATION
1.0
1.1
1.2
1.3
1.4
1.5
1.6
P/D

Fig. 5

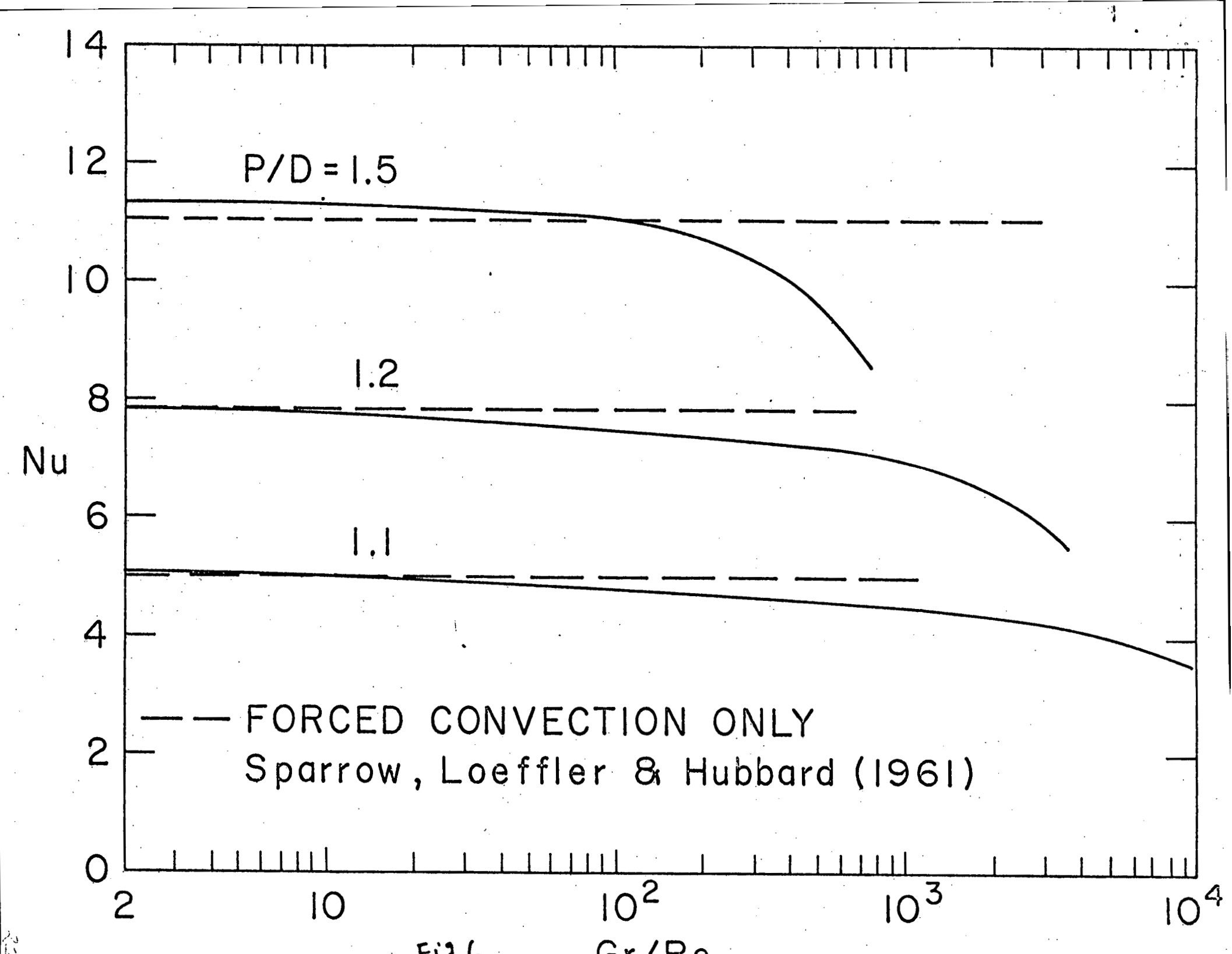
14
12
10
8
6
4
2
0
Nu
P/D = 1.5
1.2
1.1
— — FORCED CONVECTION ONLY
Sparrow, Loeffler & Hubbard (1961)
2
10
10^2
10^3
10^4
Gr/Re

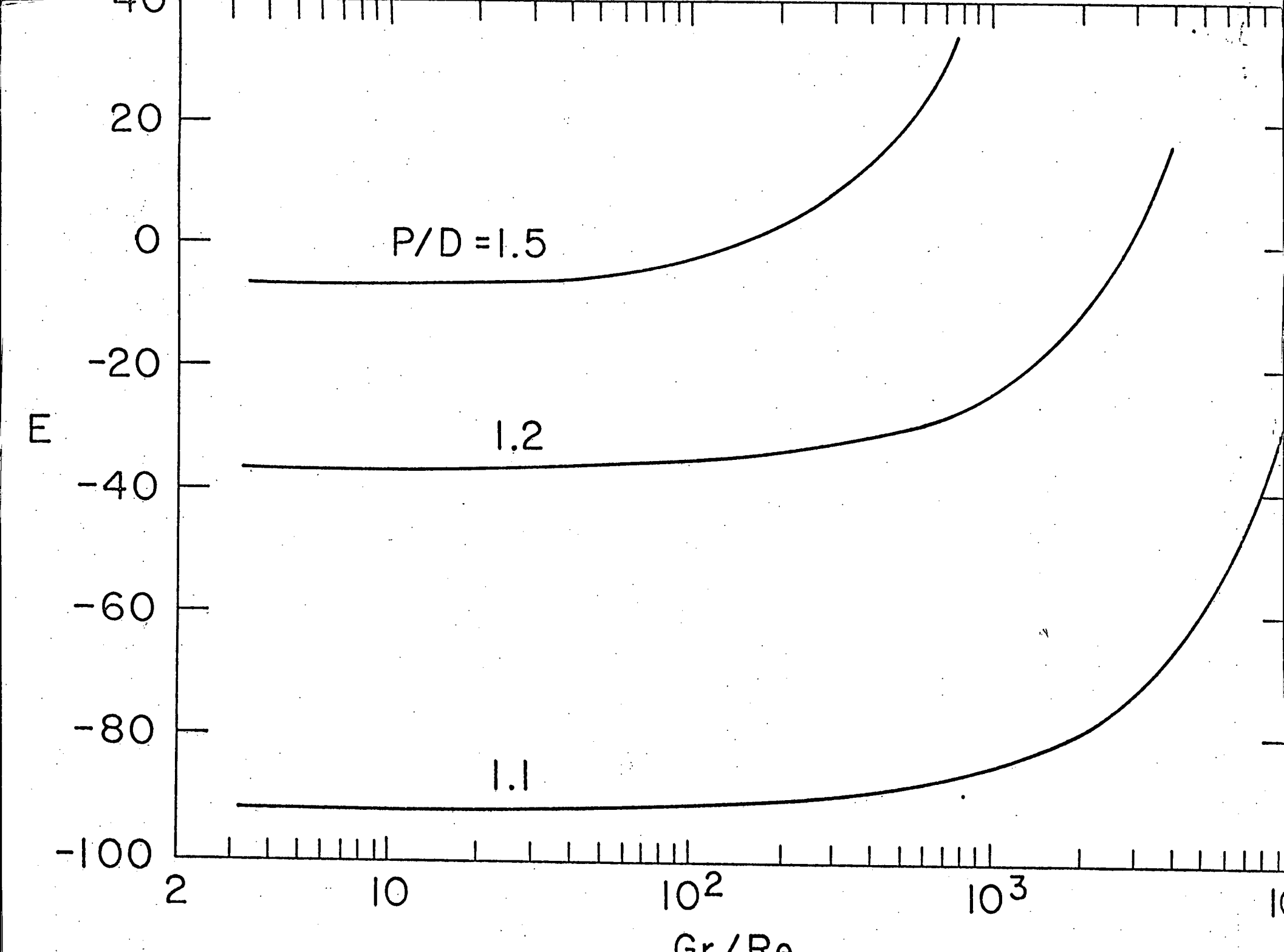

Fig. 7